

## Properties of frictional bridging in fiber pull-out for fiber-reinforced composites<sup>\*</sup>

LIU Peng-fei (刘鹏飞)<sup>†</sup>, TAO Wei-ming (陶伟明)<sup>†‡</sup>, GUO Yi-mu (郭乙木)

(Department of Engineering Mechanics, Zhejiang University, Hangzhou 310027, China)

<sup>†</sup>E-mail: Liupengfei19791226@hotmail.com; Taowm@zju.edu.cn

Received Mar. 23, 2005; revision accepted July 18, 2005

**Abstract:** Stress equilibrium equations, boundary- and continuity-conditions were used to establish a theoretical model of progressive debonding with friction at the debonded interface. On a basis of the minimum complementary energy principle, an expression for the energy release rate  $G$  was derived to explore the interfacial fracture properties. An interfacial debonding criterion  $G \geq \Gamma_i$  was introduced to determine the critical debond length and the bridging law. Numerical calculation results for fiber-reinforced composite SCS-6/Ti-6Al-4V were compared with those obtained by using the shear-lag models.

**Key words:** Fiber pull-out, Energy release rate, Bridging law, Fiber-reinforced composites

**doi:** 10.1631/jzus.2005.AS0008

**Document code:** A

**CLC number:** TG113

### INTRODUCTION

An important toughening mechanism in fiber-reinforced composites is the bridging of matrix cracks by fibers, which debond from and slide frictionally against the matrix. The magnitude of frictional sliding at the debonded interface largely affects the composite properties (Begley and McMeeking, 1995; Budiansky and Cui, 1995).

Micromechanical test of fiber pull-out has become a widely used method for exploring the properties of interfacial fracture and failure because the loads on matrix cracks exerted by fibers are pull-out loads for fibers. By testing fiber pull-out, Hampe *et al.* (1995) pointed out that a debonded interface may appear before the interfacial shear stress reaches the shear strength, which shows that the shear strength-based criterion is invalid to some extent. In contrast, the interface crack is assumed to grow when the energy release rate  $G$  exceeds the interfacial

debonding toughness  $\Gamma_i$  according to the energy-based interfacial debonding criterion, which is verified more effective than the shear strength-based criterion for exploring bridging properties (Honda and Kagawa, 1996).

It is well recognized that accurate predictions of the stress distributions in fiber and matrix are critical for determining the energy release rate and the bridging law. By applying the shear-lag models and the Lamé method respectively, Hsueh (1996) and Ochiai *et al.* (1999) obtained solutions for the energy release rate and the bridging law. However, they neglected the shear stress and strain energy in the fiber, the interfacial radial stress, the variation of axial stress in the matrix with radial positions, and the Poisson's effect. When the axial stress in the matrix is substituted by an equivalent axial stress concentrating on an effective radius, Chiang (2001) further derived an expression for the energy release rate including the axial strain energy in the fiber, and the axial and shear strain energy in the matrix. Rauchs and Withers (2002) obtained numerical solutions of the energy release rate by using the finite element method. However, oversimplifications resulted in serious errors.

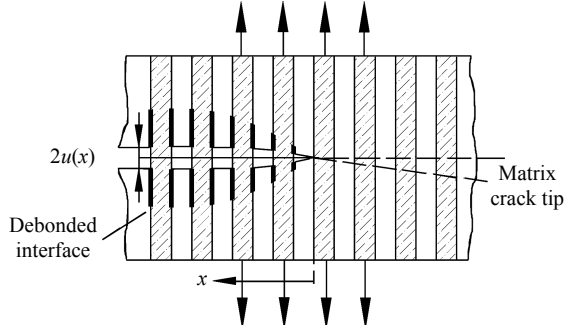
<sup>‡</sup>Corresponding author

<sup>\*</sup> Project (No. M503095) supported by the Natural Science Foundation of Zhejiang Province, China

By using stress equilibrium equations, the minimum complementary energy principle and the Euler equation, this paper first obtains stress solutions in the fiber and matrix. Based on the energy equilibrium between the work done by the pull-out stress, the work done by the friction stress, the strain energy and the interfacial energy, an expression for the energy release rate was then derived. When an interfacial debonding criterion  $G \geq \Gamma_i$  was introduced, the bridging law was finally obtained. Numerical results were compared with those obtained by Hsueh (1996) and Chiang (2001).

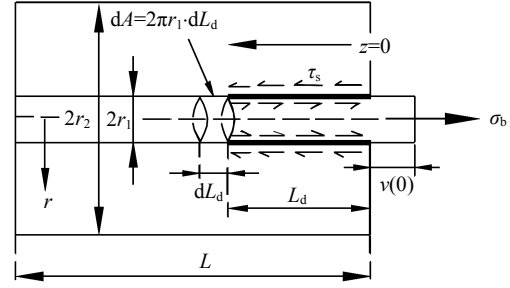
## INTERFACIAL DEBONDING CRITERIA

Fig.1 shows a composite tension specimen. An I-type matrix crack was bridged by parallel fibers at position  $x$ , a distance from the matrix crack tip. The axial displacement mismatch between the fiber and the matrix leads to the formation of the matrix crack opening displacement (COD) profile  $2u(x)$ .



**Fig.1 Schematic diagram of an I-type matrix crack bridged by parallel fibers**

A single fiber embedded in a concentric cylindrical matrix was adopted from Fig.1, as shown in Fig.2.  $r_1$  denotes the fiber radius,  $r_2$  the matrix radius,  $V_f = r_1^2 / r_2^2$  the fiber volume fraction,  $V_m = 1 - V_f$  the matrix volume fraction.  $L_d$  denotes the debond length,  $L$  the embedded fiber length. Both the fiber and matrix are considered linear-elastic. A cylindrical coordinate  $(r, \theta, z)$  is defined, with the  $z$  axis representing the fiber axial direction. The loaded and embedded ends are  $z=0$  and  $z=L$ , respectively. The pull-out stress  $\sigma_b$  is parallel to the  $z$  axis.



**Fig.2 Frictional sliding at the debonded interface under the pull-out stress**

## Stress analysis

The fiber axial stress  $\sigma_f^z(z)$  and the interfacial shear stress  $\tau_i(z)$  satisfy

$$\frac{d\sigma_f^z(z)}{dz} = -\frac{2}{r_1} \tau_i(z) \quad (1)$$

where  $\sigma_f^z(z)$  is considered as an average axial stress on the fiber cross section.

The equilibrium between the axial stresses in the fiber and matrix requires that

$$V_f \sigma_b = V_m \sigma_m^z(z) + V_f \sigma_f^z(z) \quad (2)$$

If the shear stress  $\tau_i(z)$  along the debonded interface is reduced to an average constant friction stress  $\tau_s$  resulting from the interfacial roughness effect, combining Eqs.(1) and (2) yields

$$\sigma_f^z(z) = \sigma_b - \frac{2\tau_s}{r_1} z \quad (3)$$

$$\sigma_m^z(z) = \frac{V_f}{V_m} \frac{2\tau_s}{r_1} z = \frac{2\lambda\tau_s}{r_1} z \quad (4)$$

In the cylindrical coordinate, the equilibrium equations for a 3D axisymmetric problem are given by

$$\frac{\partial \sigma^r}{\partial r} + \frac{\partial \sigma^{rz}}{\partial z} + \frac{\sigma^r - \sigma^\theta}{r} = 0 \quad (5a)$$

$$\frac{\partial \sigma^z}{\partial z} + \frac{\partial \sigma^{rz}}{\partial r} + \frac{\sigma^{rz}}{r} = 0 \quad (5b)$$

When stress functions  $\Phi_k = f_j(r)g_j(z)$  are intro-

duced according to Wu *et al.*(1998), the stress solutions satisfying Eq.(5) are expressed as

$$\begin{cases} \sigma_k^z = \frac{\partial^2 \Phi_k}{\partial r^2} + \frac{1}{r} \frac{\partial \Phi_k}{\partial r} \\ \sigma_k^{rz} = -\frac{\partial^2 \Phi_k}{\partial r \partial z} \\ \sigma_k^r = \sigma_k^\theta = \frac{\partial^2 \Phi_k}{\partial z^2} \end{cases} \quad (6)$$

where  $k=f, j=1$  and  $k=m, j=2$  represent the fiber and matrix, respectively.  $r, \theta, rz$  and  $zr$  represent the radial, circumferential and tangential directions, respectively.

Therefore, the stress solutions at the bonded regions are expressed as

$$\sigma_k^z = \left( \frac{\partial^2 f_j(r)}{\partial r^2} + \frac{1}{r} \frac{\partial f_j(r)}{\partial r} \right) g_j(z) \quad (7a)$$

$$\tau_k^{rz} = -\frac{\partial f_j(r)}{\partial r} \frac{\partial g_j(z)}{\partial z} \quad (7b)$$

$$\sigma_k^r = \sigma_k^\theta = f_j(r) \frac{\partial^2 g_j(z)}{\partial z^2} \quad (7c)$$

### Stress boundary conditions

$$\sigma_f^z(z=L_d) = \sigma_b - \frac{2\tau_s L_d}{r_1} = \sigma_d \quad (8a)$$

$$\sigma_m^z(z=L_d) = \frac{2\lambda\tau_s L_d}{r_1} \quad (8b)$$

$$\sigma_f^z(z=L) = \frac{E_f V_f}{E_c} \sigma_b \quad (8c)$$

$$\sigma_m^z(z=L) = \frac{\lambda V_m E_m}{E_c} \sigma_b \quad (8d)$$

$$E_c = V_f E_f + V_m E_m \quad (8e)$$

$$\sigma_f^r(r=r_1) = \sigma_m^r(r=r_1) \quad (8f)$$

$$\tau_f^{rz}(r=r_1) = \tau_m^{rz}(r=r_1) = \tau_i(z) \quad (8g)$$

$$\sigma_m^r(r=r_2) = 0 \quad (8h)$$

$$\tau_m^{rz}(r=r_2) = 0 \quad (8h)$$

where Eqs.(8a) and (8b) represent the continuity conditions of axial stresses in the fiber and matrix at the

crack tip  $z=L_d$ , respectively; Eqs.(8c) and (8d) represent the boundary conditions of axial stresses in the fiber and matrix at  $z=L$  (Chiang, 2001), respectively; Eqs.(8e) and (8f) represent the continuity conditions of radial and shear stresses in the fiber and matrix at  $r=r_1$ , respectively; Eqs.(8g) and (8h) represent the boundary conditions of radial and shear stresses in the matrix at  $r=r_2$ , respectively.  $\sigma_d$  is the axial stress in the fiber at  $z=L_d$  (Budiansky and Cui, 1995).  $E_k$  ( $k=f, m, c$ ) are elastic moduli of the fiber, matrix and composite, respectively.

### Stress solutions

By solving Eqs.(5b), the shear stress  $\tau_f^{rz}(r, z)$  in the fiber is obtained by

$$\tau_f^{rz}(r, z) = \frac{r}{r_1} \tau_i(z) \quad (9)$$

From Eqs.(1), (2), (5a), (8f) and Eq.(8h), the shear stress  $\tau_m^{rz}(r, z)$  in the matrix is calculated as

$$\tau_m^{rz}(r, z) = \frac{\lambda(r_2^2 - r^2)}{r_1 r} \tau_i(z) \quad (10)$$

By substituting Eq.(7a) into Eq.(8a), the functions  $f_1(r)$  and  $f_2(r)$  are then expressed as

$$f_1(r) = r^2 \sigma_d / 4 + C_1, \quad f_2(r) = C_2 r^2 + C_3 \ln r + C_4 \quad (11)$$

where  $C_q$  ( $q=1\sim 4$ ) are constant coefficients.

The relationship between the functions  $g_1(z)$  and  $g_2(z)$  is given by

$$g_2(z) = \frac{\lambda[\sigma_b - \sigma_d g_1(z)]}{4C_2} \quad (12)$$

By combining Eqs.(5), (8e)~(8h), (11) and (12), the coefficients  $C_q$  and all stresses in the fiber and matrix can be written as

$$\begin{cases} C_1 = -\frac{\sigma_d}{4} \left\{ r_1^2 + \lambda \left[ r_1^2 - r_2^2 - 2r_2^2 \ln(r_1/r_2) \right] \right\} \\ C_2 = -\lambda \frac{\sigma_d}{4}, \quad C_3 = -\lambda \frac{r_2^2 \sigma_d}{2 \ln r_2}, \quad C_4 = \lambda \frac{\sigma_d r_2^2}{4} \end{cases} \quad (13a)$$

$$\begin{cases} \sigma_f^z = \sigma_d g_1(z), \quad \tau_f^{rz} = -\frac{r\sigma_d}{2} \frac{\partial g_1(z)}{\partial z}, \\ \sigma_f^r = \sigma_f^\theta = \frac{\sigma_d}{4} \left[ r^2 - r_1^2 - \lambda(r_1^2 - r_2^2 - 2r_2^2 \ln(r_1/r_2)) \right] \frac{\partial^2 g_1(z)}{\partial z^2} \end{cases} \quad (13b)$$

$$\begin{cases} \sigma_m^z = \lambda[\sigma_b - \sigma_d g_1(z)], \\ \tau_m^{rz} = \lambda \frac{\sigma_d}{2} \left( r - \frac{r_2^2}{r} \right) \frac{\partial g_1(z)}{\partial z}, \\ \sigma_m^r = \sigma_m^\theta = -\lambda \frac{\sigma_d}{4} \left[ r^2 - r_2^2 - 2r_2^2 \ln(r/r_2) \right] \frac{\partial^2 g_1(z)}{\partial z^2} \end{cases} \quad (13c)$$

All stresses in the fiber and matrix in Eq.(13) are then determined for the function  $g_1(z)$ .

### Minimum complementary energy principle

The minimum complementary energy principle for a stable equilibrium system is expressed as: the real displacement in all possible geometric displacements always minimizes the total complementary energy  $\Pi$

$$\Pi = U_e + U_f - U_w = U_{ed} + U_{eb} + U_f - U_w \quad (14)$$

where  $U_e$  denotes the total strain energy,  $U_{ed}$  and  $U_{eb}$  are the strain energy at the debonded and bonded regions respectively,  $U_w$  is the work done by the pull-out stress  $\sigma_b$ ,  $U_f$  is the work done by the friction stress  $\tau_s$ .

The strain energy  $U_{ed}$  at the debonded regions is the sum of strain energy arising from both the pull-out stress  $\sigma_b$  and the friction stress  $\tau_s$ .

$$\begin{aligned} U_{ed} &= \int_0^{L_d} \int_0^{r_1} \left[ \frac{(\sigma_f^z(z))^2}{2E_f} + \frac{(\tau_f^{rz}(r,z))^2}{2G_f} \right] 2\pi r dr dz \\ &\quad + \int_0^{L_d} \int_{r_1}^{r_2} \left[ \frac{(\sigma_m^z(r,z))^2}{2E_m} + \frac{(\tau_m^{rz}(r,z))^2}{2G_m} \right] 2\pi r dr dz \\ &= \frac{\pi r_1^2}{2E_f} \left( \sigma_b^2 L_d - \frac{2\tau_s \sigma_b L_d^2}{r_1} + \frac{4\tau_s^2 L_d^3}{3r_1^2} \right) + \frac{\pi r_1^2 L_d \tau_s^2}{4G_f} \\ &\quad + \frac{2\pi \lambda L_d^3 \tau_s^2}{3E_m} + \frac{\pi \lambda^2 L_d \tau_s^2}{4r_1^2 G_m} \left[ 4r_2^4 \ln(r_2/r_1) + 4r_1^2 r_2^2 - r_1^4 - 3r_2^4 \right] \end{aligned} \quad (15)$$

where Eq.(15) neglects the effects of radial and circumferential stresses for simplifications.  $G$  is the shear modulus and  $G=E/[2(1+\nu)]$ .

The strain energy  $U_{eb}$  at the bonded regions is expressed as

$$U_{eb} = \sum U_{ebk} \quad (k = f, m) \quad (16)$$

$$U_{ebf} = \int_{L_d}^L \int_0^{r_1} \left[ \sigma_f^z \varepsilon_f^z / 2 + \sigma_f^r \varepsilon_f^r / 2 + \sigma_f^\theta \varepsilon_f^\theta / 2 + \tau_f^{rz} \varepsilon_f^{rz} \right] 2\pi r dr dz \quad (17a)$$

$$U_{ebm} = \int_{L_d}^L \int_{r_1}^{r_2} \left[ \sigma_m^z \varepsilon_m^z / 2 + \sigma_m^r \varepsilon_m^r / 2 + \sigma_m^\theta \varepsilon_m^\theta / 2 + \tau_m^{rz} \varepsilon_m^{rz} \right] 2\pi r dr dz \quad (17b)$$

The stress-strain relationships in the fiber and matrix are defined as

$$\begin{cases} \varepsilon_k^z = \frac{1}{E_k} [\sigma_k^z - \nu_k (\sigma_k^r + \sigma_k^\theta)] \\ \varepsilon_k^r = \frac{1}{E_k} [\sigma_k^r - \nu_k (\sigma_k^z + \sigma_k^\theta)] \\ \varepsilon_k^\theta = \frac{1}{E_k} [\sigma_k^\theta - \nu_k (\sigma_k^z + \sigma_k^r)] \end{cases} \quad (18)$$

where  $\nu$  is Poisson's ratio.

By combining Eqs.(16)~(18), the strain energy  $U_{eb}$  is calculated as

$$\begin{aligned} U_{eb} &= \frac{\pi}{2} \int_{L_d}^L \left\{ \frac{r_1^2 \sigma_d^2 g_1^2(z)}{E_f} + \frac{\lambda^2 r_1^2}{4E_m} \left[ \frac{4}{\lambda} (\sigma_b - \sigma_d g_1(z))^2 \right. \right. \\ &\quad \left. \left. + \rho r_1^2 (1 + \nu_m) \sigma_d^2 \left( \frac{\partial g_1(z)}{\partial z} \right)^2 \right] \right\} dz \end{aligned} \quad (19)$$

$$\text{where } \rho = \frac{4}{V_f^2} \ln(r_2/r_1) - \frac{3}{V_f^2} + \frac{4}{V_f} - 1.$$

The Euler-Lagrange equation for the variational complementary energy  $\Pi$  is expressed as

$$\frac{d}{dz} \left[ \frac{\partial F}{\partial g_1'(z)} \right] - \frac{\partial F}{\partial g_1(z)} = 0 \quad (20)$$

where  $F$  is the integral expression in Eq.(19).



pressed as

$$U_w = \pi r_1^2 \sigma_b U_{\text{debond}} \quad (34)$$

where  $U_{\text{debond}}$  is the additional displacement of composite due to interfacial debonding and is defined as the difference between the fiber displacement  $w_f(z)$  at the fiber loaded end  $z=0$  and composite displacement  $w_c$  in the absence of interfacial debonding

$$\begin{aligned} U_{\text{debond}} &= w_f(0) - w_c = w_f(0) - V_f \sigma_b L / E_c \\ &= \frac{\sigma_b E_m V_m L_d}{E_f E_c} - \frac{\tau_s L_d^2}{r_1 E_f} + \frac{V_m E_m \sigma_b / E_c - 2\tau_s L_d / r_1}{E_f \beta} \end{aligned} \quad (35)$$

When the interface crack with the length  $L_d$  advances a length  $dL_d$ , the interfacial energy changes by a factor  $2\pi r_1 dL_d$ . By combining Eqs.(14), (16), (19), (32) and (34), an expression for the energy release rate  $G$  is obtained as

$$G = -\frac{1}{2\pi r_1} \frac{\partial \Pi}{\partial L_d} = \lambda_1 L_d^2 + \lambda_2 L_d + \lambda_3, \quad (36)$$

$$\lambda_1 = \frac{E_c \tau_s^2}{r_1 E_f V_m E_m},$$

$$\lambda_2 = -\frac{\rho \lambda^2 r_1 \beta (1 + \nu_m) \tau_s^2}{4E_m} + \frac{3E_c \tau_s^2}{r_1 \beta E_f V_m E_m} - \frac{\sigma_b \tau_s}{E_f},$$

$$\begin{aligned} \lambda_3 &= \frac{\rho r_1^2 \lambda^2 \beta V_m (1 + \nu_m) \sigma_b \tau_s}{8E_c} - \frac{3\sigma_b \tau_s}{2E_f \beta} + \frac{r_1 E_m V_m \sigma_b^2}{4E_c E_f} \\ &+ \frac{r_1 \phi \tau_s^2}{2G_m} - \frac{\lambda^2 \tau_s^2}{8r_1^3 G_m} \left[ 4r_2^4 \ln(r_2 / r_1) + 4r_1^2 r_2^2 - r_1^4 \right. \\ &\left. - 3r_2^4 \right] - \frac{r_1 \tau_s^2}{8G_f}. \end{aligned}$$

Eq.(36) shows that the energy release rate  $G$  is a second-order function of the debond length  $L_d$  when the material and geometry parameters are known. When an interfacial debonding criterion  $G \geq \Gamma_i$  is introduced, the critical debond length can be determined by

$$L_{d1,2} = \frac{-\lambda_2 \pm \sqrt{\lambda_2^2 - 4\lambda_1(\lambda_3 - \Gamma_i)}}{2\lambda_1} \quad (37)$$

Only the smaller  $L_{d1}$  of the two roots of Eq.(37)

is physically meaningful for the reason elaborated below.

By comparisons with Eq.(36), results below were also obtained by Hsueh (1996) and Chiang (2001), respectively

$$\begin{aligned} G &= \frac{r_1 V_m E_m}{4E_f E_c} \left( \sigma_b - \frac{2\tau_s E_c L_d}{r_1 V_m E_m} \right)^2 \\ &= \frac{E_c \tau_s^2}{r_1 E_f V_m E_m} L_d^2 - \frac{\sigma_b \tau_s}{E_f} L_d + \frac{r_1 E_m V_m \sigma_b^2}{4E_c E_f} \end{aligned} \quad (38)$$

$$\begin{aligned} G &= \frac{E_c \tau_s^2}{r_1 E_f V_m E_m} L_d^2 + \left( \frac{E_c \tau_s^2}{\eta E_f V_m E_m} - \frac{\sigma_b \tau_s}{E_f} \right) L_d \\ &+ \frac{r_1 E_m V_m \sigma_b^2}{4E_c E_f} - \frac{r_1 \sigma_b \tau_s}{2\eta E_f} \end{aligned} \quad (39)$$

$$\eta^2 = \frac{4E_c G_m}{V_m E_m E_f \phi} \quad (40)$$

According to McCartney (2005), for the bridging fibers in the process of matrix crack growth, the bridging law is defined as the relationship between the bridging traction  $T(x)$  and the half COD profile  $u(x)$ . By substituting Eq.(37) into (31), the bridging law is obtained as

$$v(0) = -\frac{\tau_s E_c}{r_1 E_f E_m V_m} L_{d1}^2 + \left( \frac{\sigma_b}{E_f} - \frac{2\tau_s E_c}{r_1 \beta E_f E_m V_m} \right) L_{d1} + \frac{\sigma_b}{\beta E_f} \quad (41)$$

$$u = \frac{E_m V_m}{E_c} v(0), \quad T(x) = \sigma_b(x) V_f \quad (42)$$

By comparison with Eq.(41), the result below was also obtained by Hsueh (1996)

$$v(0) = \frac{r_1 V_m E_m \sigma_b^2}{4E_f E_c \tau_s} - \frac{\Gamma_i}{\tau_s} \quad (43)$$

## RESULTS AND DISCUSSION

Fiber-reinforced composite SCS-6/Ti-6Al-4V is adopted for numerical calculations. Material parameters:  $E_f = 400$  GPa,  $E_m = 400$  GPa,  $\nu_f = 0.17$ ,  $\nu_m = 0.3$  (Preuss *et al.*, 2003). The fiber tensile strength  $\sigma_s = 4.19$  GPa (Warrier *et al.*, 1999). The fiber

radius is  $r_1=10 \mu\text{m}$  and the fiber volume fraction is  $V_f=1\%$ .

Fig.3 shows distributions of the energy release rate  $G$  via the normalized debond length  $L_d/r_1$ . Theoretically, the friction stress  $\tau_s$  contributes to  $G$  in the form of  $E_c \tau_s^2 / (r_1 E_f V_m E_m)$  in Eqs.(36), (38) and (39), yielding the first decreasing and then re-increasing tendency with the increase of  $L_d/r_1$ . However, the re-increasing part is physically meaningless because interfacial debonding appears only at  $G > \Gamma_i$  (here, the interfacial debonding toughness is assumed as  $\Gamma_i=1 \text{ J/m}^2$ ) and stops after the condition  $G=\Gamma_i$  is satisfied. Therefore, the critical debond length is taken as the smaller one  $L_{d1}$  in Eq.(37), which was also verified by Liu and Kagawa (2000) whose conclusions were based on the Lamé solutions and suffered from similar setbacks like those in the shear-lag models. The values for  $G$  obtained by us are smaller than those obtained by Hsueh (1996) and Chiang (2001) because Hsueh neglected the shear stress and strain energy in the fiber and matrix, the radial stresses in the fiber and matrix, the variation of axial stress in the matrix with radial positions, and the Poisson's effect. Chiang considered only the shear stress in the matrix.

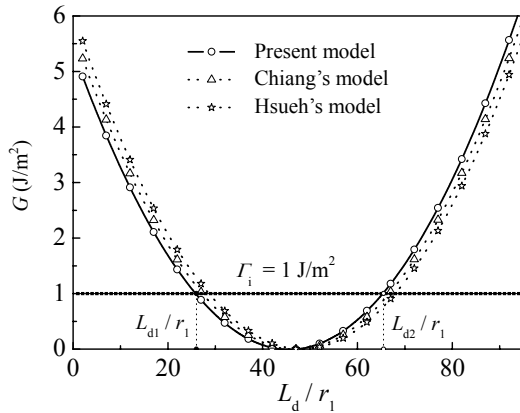


Fig.3 Distributions of the energy release rate  $G$  via the normalized debond length  $L_d/r_1$  at the pull-out stress  $\sigma_b=1 \text{ GPa}$  and the friction stress  $\tau_s=10 \text{ MPa}$

Fig.4 illustrates the effect of friction stress  $\tau_s$  on the energy release rate  $G$ . Increasing friction stress  $\tau_s$  results in smaller  $G$  at the same  $L_d/r_1$ , improving the interfacial debonding toughness  $\Gamma_i$ . The curves  $G \sim L_d/r_1$  tend to be smooth when the friction stress  $\tau_s$  decreases and approaches the minimum value  $\tau_s=0$ , where the energy release rate reaches the maximum

value  $G=6.02 \text{ J/m}^2$  for the decreasing parts of curves.

Fig.5 shows the bridging law between the bridging traction  $T(x)$  and the half COD profile  $u(x)$ . The values for  $T(x)$  are slightly smaller than those obtained by Hsueh (1996) at the same  $u(x)$ , showing a stronger ability to resist the interface failure. The shear effects in the fiber and matrix and Poisson's effect neglected by the shear-lag models become more remarkable with the increase of friction stress  $\tau_s$ , which is also directly concluded from Eq.(36).

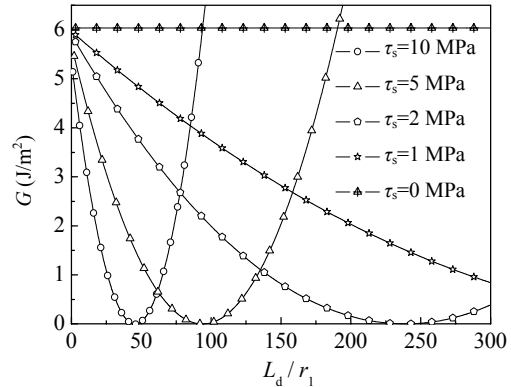


Fig.4 Distributions of the energy release rate  $G$  via the normalized debond length  $L_d/r_1$  at the pull-out stress  $\sigma_b=1 \text{ GPa}$  and the friction stress  $\tau_s=0, 1, 2, 5, 10 \text{ MPa}$ , respectively

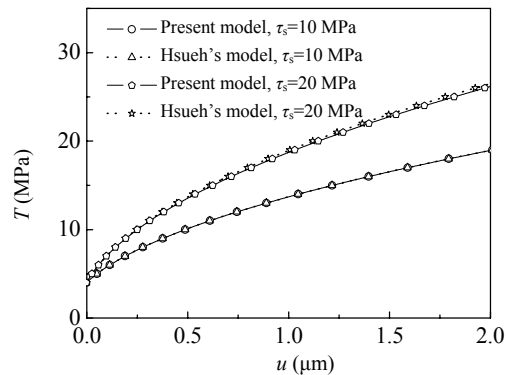
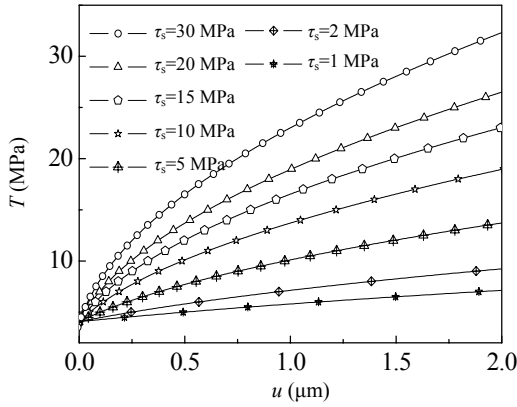


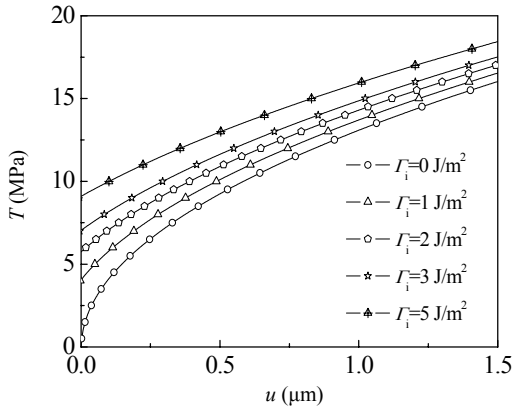
Fig.5 The bridging law at the interfacial debonding toughness  $\Gamma_i=1 \text{ J/m}^2$  and the friction stress  $\tau_s=10, 20 \text{ MPa}$ , respectively

Fig.6 illustrates the effect of friction stress  $\tau_s$  on the bridging law. The bridging traction  $T(x)$  is independent of the half COD profile  $u(x)$  at  $\tau_s=0$  and increasing  $\tau_s$  results in larger  $T(x)$  at the same  $u(x)$ .

Fig.7 shows the effect of interfacial debonding toughness  $\Gamma_i$  on the bridging law. The curves  $T(x) \sim u(x)$  start at the origin at  $\Gamma_i=0$  and approach a plateau



**Fig. 6** The bridging law at the interfacial debonding toughness  $\Gamma_i=1 \text{ J/m}^2$  and the friction stress  $\tau_s=1, 2, 5, 10, 15, 20, 30 \text{ MPa}$ , respectively



**Fig. 7** The bridging law at the friction stress  $\tau_s=10 \text{ MPa}$  and the interfacial debonding toughness  $\Gamma_i=0, 1, 2, 3, 5 \text{ MPa}$ , respectively

level with the increase of  $\Gamma_i$ . Increasing  $\Gamma_i$  results in larger  $\Gamma_i$  at the same  $u(x)$ .

The bridging law for determining the bridging traction  $T(x)$  obtained from the half COD profile  $u(x)$  in terms of the frictional bridging can be expressed as (Marshall and Cox, 1998)

$$T(x) = a + bu(x)^n \tag{44}$$

where the coefficients  $a, b, n$  are constants related to the material parameters, the fiber volume fraction, the interfacial properties, etc.

Marshall and Cox (1998) found the power exponent  $n=0.5$  by combining the bridging traction  $T(x)$  and the half COD profile  $u(x)$  based on a force balance between the external tensile stress and the in-

ternal bridging stress.

By fitting a series of discrete data, the power exponents are calculated as  $n=0.50327, 0.50327, 0.50327, 0.5033, 0.50335, 0.50343$  and  $0.50365$  at the friction stress  $\tau_s=1, 2, 5, 10, 15, 20, 30 \text{ MPa}$  respectively in Fig.6;  $n=0.50838, 0.5033, 0.49822, 0.49314$  and  $0.48296$  at the interfacial debonding toughness  $\Gamma_i=0, 1, 2, 3, 5 \text{ J/m}^2$  respectively in Fig.7.

Eqs.(36), (37), (41) and (42) show that the interrelationship between the bridging traction  $T(x)$  and the half COD profile  $u(x)$  becomes weaker at  $\tau_s \rightarrow 0$  and is equal to zero at  $\tau_s=0$ , corresponding to the case of no bridging. However, more axial and shear deformations occur and more fibers break in a strong interface with high friction stress  $\tau_s$ , causing the power exponent to deviate from the value  $n=0.5$ . Therefore, the power law relationship  $n=0.5$  is more acceptable in the case of a weak interface with relatively low friction stress  $\tau_s$  and interfacial debonding toughness  $\Gamma_i$  than in a strong interface case.

### CONCLUSION

A theoretical model of progressive debonding with friction at the debonded interface was established by introducing stress equilibrium equations, and boundary- and continuity-conditions. The solutions for the energy release rate  $G$  and the bridging law were obtained based on the minimum complementary energy principle. Our study results on the effects of various parameters on fiber-reinforced composite SCS-6/Ti-6Al-4V compared with those obtained by existing models. The following conclusions were reached:

- (1) Our proposed method for determining the critical debond length  $L_d$  by introducing an interfacial debonding criterion  $G \geq \Gamma_i$  is feasible;
- (2) When the friction stress  $\tau_s$  decreases, the curves  $G \sim L_d/r_1$  tend to be smooth until  $G$  becomes a constant independent of the debond length  $L_d$  at  $\tau_s=0$ ;
- (3) Theoretically, the curves  $G \sim L_d/r_1$  have the first decreasing and then re-increasing tendency. However, the re-increasing part is physically meaningless because interfacial debonding appears only at  $G > \Gamma_i$  and stops after the condition  $G = \Gamma_i$  is satisfied;
- (4) The shear effects in the fiber and matrix and Poisson's effect neglected by the shear-lag models become more remarkable with the increase of friction



stress  $\tau_s$  for suppressing the interface failure;

(5) The power exponent  $n=0.5$  in the bridging law is more acceptable in the case of a weak interface with low friction stress  $\tau_s$  and interfacial debonding toughness  $\Gamma_i$  than in a strong interface case.

## References

- Begley, M.R., McMeeking, R.M., 1995. Numerical analysis of fibre bridging and fatigue crack growth in metal matrix composite materials. *Materials Science and Engineering*, **200**(1-2):12-20.
- Budiansky, B., Cui, Y.L., 1995. Toughening of ceramics by short aligned fibers. *Mechanics of Materials*, **21**(2):139-146.
- Chiang, Y.C., 2001. On fiber debonding and matrix cracking in fiber-reinforced ceramics. *Composites Science and Technology*, **61**(12):1743-175.
- Hampe, A., Kalinka, G., Meretz, S., 1995. An advanced equipment for single-fibre pull-out test designed to monitor the fracture process. *Composites*, **26**(1):40-46.
- Honda, K., Kagawa, Y., 1996. Debonding criterion in the pushout process of fiber-reinforced ceramics. *Acta Materialia*, **44**(8):3267-3277.
- Hsueh, C.H., 1996. Crack-wake interfacial debonding criteria for fiber-reinforced ceramic composites. *Acta Materialia*, **44**(6):2211-2216.
- Liu, Y.F., Kagawa, Y., 2000. The energy release rate for an interfacial debond crack in a fiber pull-out model. *Composites Science and Technology*, **60**(2):167-171.
- Marshall, M.B., Cox, B.N., 1998. A-J-integral method for calculating steady-state matrix cracking stresses in composites. *Mechanics of Materials*, **17**(1):127-136.
- McCartney, L.N., 2005. Energy-based prediction of failure in general symmetric laminates. *Engineering Fracture Mechanics*, **72**(6):909-930.
- Ochiai, S., Hojo, M., Inoue, T., 1999. Shear-lag simulation of the progress of interfacial debonding in unidirectional composites. *Composites Science and Technology*, **59**(1):77-88.
- Preuss, M., Rauchs, G., Doel, T.J.A., 2003. Measurements of fibre bridging during fatigue crack growth in Ti/SiC fibre metal matrix composites. *Acta Materialia*, **51**(4):1045-1057.
- Rauchs, G., Withers, P.J., 2002. Computational assessment of the influence of load ratio on fatigue crack growth in fibre-reinforced metal matrix composites. *International Journal of Fatigue*, **24**(12):1205-1211.
- Warrier, S.G., Maruyama, B., Majumdar, B.S., 1999. Behavior of several interfaces during fatigue crack growth in SiC/Ti-6Al-4V composites. *Materials Science and Engineering*, **259**(2):189-200.
- Wu, W., Verpoest, I., Varna, J., 1998. A novel axisymmetric variational analysis of stress transfer into fibres through a partially debonded interface. *Composites Science and Technology*, **58**(12):1863-1877.

Welcome visiting our journal website: <http://www.zju.edu.cn/jzus>

Welcome contributions & subscription from all over the world

The editor would welcome your view or comments on any item in the journal, or related matters

Please write to: Helen Zhang, Managing Editor of JZUS

E-mail: [jzus@zju.edu.cn](mailto:jzus@zju.edu.cn) Tel/Fax: 86-571-87952276